Comparison of frequency-resolved optical polarization gating induced by molecular alignment and Kerr effects

Jia Liu, Wenxue Li, Hao Li, Yahui Feng, Haifeng Pan, Jian Wu, and Heping Zeng*

State Key Laboratory of Precision Spectroscopy, East China Normal University, Shanghai 200062, China
**Corresponding author: hpzeng@phy.ecnu.edu.cn*

Received April 24, 2012; accepted May 21, 2012;
posted May 24, 2012 (Doc. ID 167293); published June 28, 2012

We experimentally demonstrated that both the electronic Kerr effect and the molecular alignment in gaseous molecules could be applied as transient gates to diagnose 400 nm target pulses. Their birefringence dissimilarity was clearly visualized by the measured spectrogram and retrieved gate function. In the atomic gas argon, a relatively weak and instantaneous cross phase modulation within the pulse duration was observed, while in the molecular gas N_2, the delayed rotational Raman excitation played a dominative role. © 2012 Optical Society of America

OCIS codes: 320.7100, 190.7110, 320.7160.

Field-free alignment of gaseous molecules by impulsive rotational Raman excitation and its periodic revivals have been extensively applied in generating transient birefringence [1], fixing molecules [2,3], ultrafast molecular buffer [4,5], and controlling the propagation of laser pulses [6,7]. Very recently, ultrafast polarization optical gating, with periodic revivals by molecular alignment, was successfully applied in molecular alignment based cross-correlation frequency-resolved optical gating (M-XFROG) for measurements of ultrashort ultraviolet [8] and supercontinuum pulses [9] and molecular alignment based optical imaging and buffered storage [4]. Compared with conventional polarization-gate (PG) FROG and other FROG geometries that exploit nonlinear frequency mixing processes, M-XFROG makes use of ultrafast optical polarization gating with periodic revivals originated from quantum wakes of the impulsively excited molecular wave-packets [8,9]. Transient birefringence of the aligned gaseous molecules induces a linear polarization rotation and "real" gate function without complex phase. As a result, the M-XFROG exhibits several advantages, such as no phase-matching constraint and applicability to pulses at any wavelength ranging from ultraviolet to far-infrared.

Nevertheless, molecular alignment based polarization gating becomes complicated around the excitation time of the aligning pump pulses, since optical Kerr effects are involved during this period in gating the weak probe pulses by nonlinear coupling with the strong aligning pump pulses. Thus, the FROG measurements require to distill polarization gating of different origins. Although Kerr effect induced ultrafast transient birefringence could also be used to realize a PG-FROG, it is critically dependent on the strong excitation pulses [10,11]. Such an instantaneous gating is originated from Kerr induced changes of nonlinear refractive index within the pump pulse duration that differentiate parallel and orthogonal to the pump field polarization, while molecular optical gating exhibits a delayed response due to the rotational Raman excitation of molecules. Accordingly, molecular alignment together with Kerr effects generate temporally broadened optical gating of different mechanisms, which seem to complicate the FROG diagnosis of ultrashort pulses.

In this Letter, we compared the role of the Kerr effect and molecular alignment induced birefringence in molecular N_2 on the measurement of ultrashort laser pulses. Our result indicated that either Kerr or molecular alignment could be utilized to characterize unknown laser pulses, while the molecular alignment was the dominative one for molecular gas and showed a very high signal-to-noise ratio. Moreover, the dissimilarity between such two phenomena and their independent contributions to the gate function were clarified by simply comparing the measured FROG traces and retrieved gates, which were consistent with the molecular alignment induced spatial (de)focusing measurements [12].

The experiment was performed with a Ti:sapphire laser system delivering 50 fs laser pulse at 800 nm, which was split into an excitation and a probe pulse. The excitation pulse was used to generate Kerr effect or align molecules, while the probe passed through a β barium borate (BBO) crystal (type I, 29.2 deg cut, 100 μm thick) to produce a frequency-doubled 400 nm target pulse. The two pulses were then collinearly combined and focused ($f = 60$ cm) into a gas cell filled with 0.8 bar argon or N_2. The polarization of the excitation pulse was set to be 45 deg with respect to the target pulse to achieve a maximal polarization modulation. The transient birefringence induced polarization change was extracted by an ultrahigh contrast polarizer (distinction ratio $\sim 10^6:1$), whose transmission direction was set orthogonal to the polarization direction of the target pulse. The FROG trace was formed by recording the time-resolved transmitted spectra by a fiber-coupled spectrometer (Ocean optics, HR4000). The measured FROG trace was preprocessed to minimize noise by a background subtraction and Fourier domain filtering algorithm and then interpolated to a square matrix [8], which was then used for temporal intensity and phase retrieval.

Figure 1 shows the comparison of the results from the Kerr effect based PG-FROG and the M-XFROG under the same excitation intensity of 3.8×10^{13} W/cm^2. Both FROG traces were retrieved by using the twin retrieval of the excitation electric fields (TREEFROG) algorithm [13]. Figures 1(a) and 1(b) show the measured FROG traces by using molecular N_2 and atomic Ar gases,

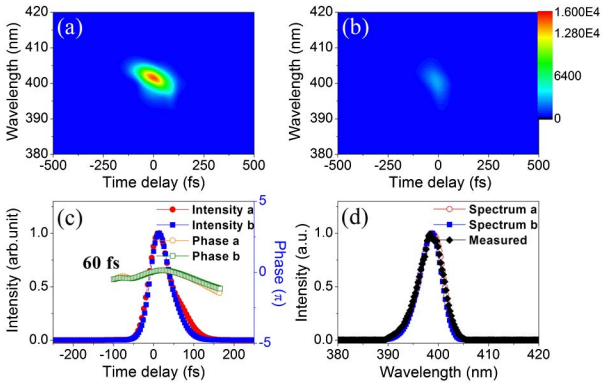

Fig. 1. (Color online) The measured FROG traces in the case of (a) N_2. (b) Ar under the excitation intensities of 3.8×10^{13} W/cm^2. (c) The retrieved temporal intensity (red-circular, blue-squared) and phase (orange-circular, green squared). (d) The reconstructed (red-circular, blue-squared) and measured (black-diamond) spectrum.

respectively. Similarly sloped spectra were revealed. The main differences came from the peak intensity and temporal width. A better signal-to-noise ratio was obtained in the M-XFROG as its peak intensity was about six times to that of the Ar based PG-FROG. The relative root-mean-square error between the measured and retrieved traces was less than 0.3% after 300 iterations [14,15]. Figures 1(c) and 1(d) show the corresponding reconstructed pulse intensity, phase and spectra. The quadratic phase in Fig. 1(c) clearly indicates a positive chirp pulse structure as we could also intuitively deduce from the FROG traces. Apart from some minor differences in the tailoring part, the retrieved intensities and phases in these two cases were almost the same. The measured (black-diamond) and reconstructed spectrum (red-circular, blue-squared) are shown in Fig. 1(d). The agreement is excellent and the retrieval algorithm precisely retells the shape and bandwidth of the probe pulse spectrum.

We then investigated the FROG trace variation in Ar and N_2 under different excitation intensities of 1.1×10^{13}, 2.1×10^{13}, and 3.8×10^{13} W/cm^2, as shown in Figs. 2(a) and 2(b). The corresponding integration of the measured FROG traces over all spectra, considered as the intensity cross correlation signal, are illustrated in Fig. 2(c). We could observe a sensitive increase of the correlation signal by increasing the excitation intensity in both cases. Moreover, the counterpart correlation intensity in Ar was much smaller than that in N_2 under the same excitation condition, such as (a)iii and (b)iii in Fig. 2(c), indicating that the Kerr effect induced birefringence was much smaller than that induced by molecular alignment, which was clearly shown by the corresponding contour plots of the FROG traces in Figs. 2(a) and 2(b)iii. Such a dissimilarity became even more observable under low intensity excitation as shown in Figs. 2(a) and 2(b)i, where we could hardly discriminate the FROG trace induced by Ar from its background while the FROG trace by N_2 was distinguishable and exhibited a much better signal-to-noise ratio, which could be potentially applied in the low intensity regime and enable us to get more reliable results.

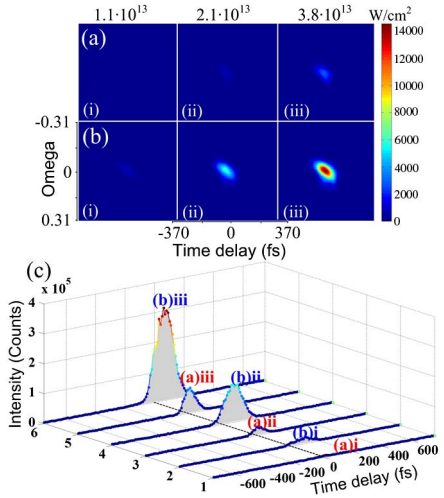

Fig. 2. (Color online) (a) The measured FROG traces in (a) Ar and (b) N_2 under different excitation intensities of 1.1×10^{13}, 2.1×10^{13}, and 3.8×10^{13} W/cm^2. (c) The corresponding intensity cross correlation signals of the measured FROG traces in (a) and (b).

The TREEFROG retrieval algorithm [13] enables us to simultaneously reconstruct the target and gate pulses and provides a valid way to distinguish the Kerr effect from the molecular alignment. Note that the gate function is related to the refractive index change δn. The Kerr effect produces a refractive index change along the excitation polarization axis as $\delta n_{\mathrm{Kerr}\parallel} = n_2 I$, while the perpendicular component is $\delta n_{\mathrm{Kerr}\perp} = 1/3\delta n_{\mathrm{Kerr}\parallel}$. The molecular alignment degree is characterized by the metric $\langle\langle \cos^2\theta\rangle\rangle$ and the prealigned molecules show orientation-dependent refractive index changes as $\delta n_{\mathrm{rot}} = 3/4(\rho_0 \Delta\alpha/n_0)(\langle\langle \cos^2\theta\rangle\rangle - 1/3)$ [16], where ρ_0 is the initial molecule density, $\Delta\alpha = \alpha_\parallel - \alpha_\perp$ is the polarizability anisotropy between the components parallel and perpendicular to the molecular axis, n_0 is the linear refractive index of the randomly orientated molecules, θ is the angle between the molecule axis and field polarization. The total refractive index change is the sum of the electronic Kerr and molecular alignment, given as $\delta n = 3(\rho_0 \Delta\alpha/n_0)(\langle\langle \cos^2\theta\rangle\rangle - 1/3) + 2/3 n_2 I$.

The retrieved gate functions a (squared) and b (circular curve) in the case of N_2 and Ar are presented in Fig. 3(a), from which we could see that molecular alignment induced gate was much more intense (1∶0.42) and wider than that (Gate b) induced by Kerr

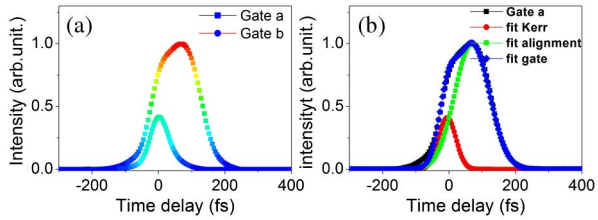

Fig. 3. (Color online) (a) The retrieved gate functions a (squared curve) and (b) (circular curve) related to the case of N_2 and argon under the excitation intensities of 3.8×10^{13} W/cm^2. (b) The Gaussian fit of Gate a, with distinguishable contributions from Kerr effect (red-circular curve) and molecular alignment (green-squared curve).

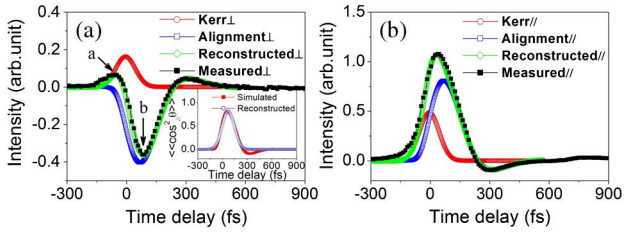

Fig. 4. (Color online) Spatial (de)focusing effects based measurement of molecular alignment signal (black-squared curve) under the excitation intensity of 3.8×10^{13} W/cm^2 by (a) perpendicularly and (b) parallel polarized weak probe. Inset: the comparison of the reconstructed and simulated alignment signals around zero delay.

effect. The zero time delay was set as the peak of the FROG trace in argon gas since the maximum electronic Kerr cross phase modulation was reached as the excitation and target pulses were temporally overlapped. According to the Gaussian fit of the gate function a of N_2, as shown in Fig. 3(b), the first red-circular peak centered around zero delay was the contribution from the Kerr effect within the pulse duration (FWHM = 70 fs), while the impulsive rotational response (green-squared) was delayed by ~80 fs. Meanwhile, the intensity of Gate b and the fitted Kerr effect of N_2 was approximately equal, indicating that the nonlinear refractive indexes n_2 of Ar and N_2 were similar, which was consistent with recent measurements [16] $n_2 = 0.22 \pm 0.04$ and 0.20 ± 0.02 cm^2/EW for N_2 and Ar, respectively. Although both the molecular alignment and Kerr effects were involved in the M-XFROG measurement, their collaboration still enables a clean single-peak gate function and smooth FROG trace. Moreover, the independent contribution to the gate function could be simply distinguished with the method described above.

The electronic Kerr effect and molecular alignment were further distinguished by measuring the spatial (de)focusing of the probe pulse [12]. By extracting the spatial intensity modulation of a weak probe pulse caused by the spatial refractive index gradient, the molecular alignment signal could be directly reconstructed. Figure 4(a) shows the measured alignment signal (black-squared curve) around zero delay under the same excitation intensity as the probe pulse was orthogonally polarized to that of the pump, accompanied with the reconstructed result from M-XFROG (green-diamond curve) by considering the certain value of each effect. The probe pulse was firstly focused by Kerr self-focusing around zero time delay (red-circular curve) within the pulse duration, leading to a positive signal (marked with arrow a), whereas the molecular alignment induced cross-defocusing after ~100 fs (blue-squared curve) gave rise to a negative valley signal (marked with arrow b). However, a preceding (~54 fs to that of the zero delay), suppressed weaker focusing (3/8 of the single Kerr) and delayed defocusing (~18 fs) were aroused by the collaborated effect of Kerr and molecular alignment. This provides a way to control the propagation of an intense laser pulse, such as the formation and collapse of a filament and supercontinuum generation. The inset of Fig. 4(a) presents the reconstructed and simulated alignment signals (N_2, 50 fs, 800 nm, 3.8×10^{13} W/cm^2) with an obvious difference around 300 fs. Note that the reconstructed alignment signal is all positive due to the nonnegative property of FROG trace. We used simulated alignment (green-squared curve) in reconstructing the intensity modulation signal. The measured and reconstructed alignment with a parallel polarized probe pulse are shown in Fig. 4(b). The reconstruction was taken from Fig. 4(a) by considering the relationship of the parallel and perpendicular components of the refractive index changes. A good quantitative agreement between the experimental and reconstructed results confirmed the reliability of the M-XFROG technique.

In summary, we demonstrated that both Kerr and molecular alignment could be applied to characterize unknown ultrashort laser pulses and that M-XFROG could distinguish instantaneous Kerr and delayed rotational effects. This was confirmed by direct measurement and reconstruction of spatial (de)focusing effects around zero time delay.

This work was partly funded by National Natural Science Fund (10990101 & 11004061), National Key Project for Basic Research (2011CB808105), and International Science and Technology Cooperation Program of China (2010DFA04410).

References

1. H. Stapelfeldt and T. Seideman, Rev. Mod. Phys. **75**, 543 (2003).
2. J. Itatani, J. Levesque, D. Zeidler, H. Niikura, H. Pépin, J. C. Kieffer, P. B. Corkum, and D. M. Villeneuve, Nature **432**, 867 (2004).
3. R. Velotta, N. Hay, M. B. Mason, M. Castillejo, and J. P. Marangos, Phys. Rev. Lett. **87**, 183901 (2001).
4. J. Wu, P. Lu, J. Liu, H. Li, H. Pan, and H. Zeng, Appl. Phys. Lett. **97**, 161106 (2010).
5. E. Hertz, B. Lavorel, and O. Faucher, Nat. Photon. **5**, 78 (2011).
6. S. Varma, Y.-H. Chen, and H. M. Milchberg, Phys. Rev. Lett. **101**, 205001 (2008).
7. J. Wu, Y. Tong, X. Yang, H. Cai, P. Lu, H. Pan, and H. Zeng, Opt. Lett. **34**, 3211 (2009).
8. P. Lu, J. Liu, H. Li, H. Pan, J. Wu, and H. Zeng, Appl. Phys. Lett. **97**, 061101 (2010).
9. J. Liu, Y. Feng, H. Li, P. Lu, H. Pan, J. Wu, and H. Zeng, Opt. Express **19**, 40 (2011).
10. R. Trebino and D. J. Kane, J. Opt. Soc. Am. A **10**, 1101 (1993).
11. P. Béjot, Y. Petit, L. Bonacina, J. Kasparian, M. Moret, and J. P. Wolf, Opt. Express **16**, 7564 (2008).
12. Y. Feng, H. Pan, J. Liu, C. Chen, J. Wu, and H. Zeng, Opt. Express **19**, 2852 (2011).
13. K. W. De Long, R. Trebino, and W. E. White, J. Opt. Soc. Am. B **12**, 2463 (1995).
14. K. W. De Long, D. N. Fittinghoff, and R. Trebino, IEEE J. Quantum Electron. **32**, 1253 (1996).
15. D. N. Fittinghoff, K. W. De Long, R. Trebino, and C. L. Ladera, J. Opt. Soc. Am. B **12**, 1955 (1995).
16. V. Loriot, E. Hertz, O. Faucher, and B. Lavorel, Opt. Express **17**, 13429 (2009).